fluids

MDPI

Article

Numerical Simulation of First-Order Surface Reaction in Open Cavity Using Lattice Boltzmann Method

Cristian Yoel Quintero-Castañeda [1], María Margarita Sierra-Carrillo [1], Arturo I. Villegas-Andrade [1] and Javier Burgos-Vergara [2,*]

[1] Faculty of Engineering, Universidad Cooperativa de Colombia, Santa Marta 470003, Colombia; cristian.quinteroc@campusucc.edu.co (C.Y.Q.-C.); mariam.sierra@campusucc.edu.co (M.M.S.-C.); arturo.villegasa@campusucc.edu.co (A.I.V.-A.)
[2] Faculty of Engineering, Coorporación Universitaria Reformada, Barranquilla 080016, Colombia
* Correspondence: j.burgos@unireformada.edu.co; Tel.: +57-605-3226100

Abstract: The lattice Boltzmann method (LBM) is a finite element and finite volume method for studying the reaction rate, mass diffusion and concentration of species. We are used the LBM to investigate the effect of the Damköhler number (Da) and Reynolds number (Re) on the laminar flow in a channel with an open square cavity and a reactive bottom wall in two dimensions in a first-order chemical reaction. The reactant A is transported through the cavity, where it undergoes a reaction on the reactive surface, resulting in the synthesis of product B. The effect of Da < 1 on the reaction rate is negligible for all investigated Re values; the generation of product B is slower because of the effect of the momentum diffusivity on the velocity inside the cavity. For Re = 5 and 1 < Da $\leq$ 100, the concentration of B inside the cavity reaches the maximum for Da = 100, and A is absorbed almost entirely on the bottom of the cavity. In our simulations, we observed that for all values of Re and Da > 100, the effect of the momentum diffusivity is negligible in the cavity, and the reaction on the surface is almost instantaneous.

Keywords: lattice Boltzmann; numerical simulation; surface reaction; Damköhler number; Reynolds number; computational fluid dynamics

check for updates

Academic Editors: Jie Bao and Leonardo Santos de Brito Alves

Received: 21 September 2024
Revised: 23 November 2024
Accepted: 3 December 2024
Published: 30 December 2024

Citation: Quintero-Castañeda, C.Y.; Sierra-Carrillo, M.M.; Villegas-Andrade, A.I.; Burgos-Vergara, J. Numerical Simulation of First-Order Surface Reaction in Open Cavity Using Lattice Boltzmann Method. *Fluids* **2025**, *10*, 7. https://doi.org/10.3390/fluids10010007

Copyright: © 2024 by the authors. Licensee MDPI, Basel, Switzerland. This article is an open access article distributed under the terms and conditions of the Creative Commons Attribution (CC BY) license (https://creativecommons.org/licenses/by/4.0/).

1. Introduction

The lattice Boltzmann method (LBM) has become a powerful alternative to the finite element and finite volume methods for solving different problems in various engineering applications [1], including heat and mass transfer problems for single and multiphase flow, blood flow, compressible flows and magnetodynamics and chemical reaction problems [2–5]. In the present work, the LBM is used to study the problem of a first-order chemical reaction in an open cavity with a reaction bottom wall. This geometry represents a microreactor with a simple reaction flow with a chemical reaction in the bottom of the cavity. In recent years, the LBM has been used as a solution method for different problems related to heat and mass transfer processes [6–9].

To validate the applicability of the LBM in two dimensions to certain phenomena related to mass transfer processes, we conducted two simulations in the steady-state regime for an incompressible fluid flow: for advection–diffusion, a Gaussian pulse was used to validate the first case using the single-relaxation-time (SRT) LBM [10] and the multiple-relaxation-time (MRT) LBM [11,12].

The Gaussian pulse problem refers to the evolution of an initial concentration pulse inside a rectangular domain with dimensionless length; the initial Gaussian pulse is advected

with constant velocity in a diagonal line across the domain [13]. We compared the analytical solution for the Gaussian pulse with the LBM results for the two different grid sizes and for the MRT and SRT models [14,15]. A deviation with respect to the analytic solution was observed, with a larger relative error (ε = 0.86%) observed for a larger resolution grid when the SRT model was used [16]. An improvement was achieved using the MRT model, resulting in a substantial improvement in the relative error in the final peak concentration (ε = 0.10%) compared with that predicted by the SRT model [17].

Another simulation was carried out: the Lévêque problem for mass flux. The Lévêque problem is a simple case of an analysis of the mass transfer through a reactive surface (plate), where an engineering application is comparable to a chemical catalysis reaction [18]. This problem consists of a two-dimensional Poiseuille flow fully developed in a laminar region, with a constant concentration at the entrance of the channel. In the Lévêque problem, in the region of the catalytic surface, the reaction is assumed to be infinitely fast. The Sherwood number Sh as a function of the Péclet number Pe, the reference values reported by Holzbecher [19] and the COMSOL 5.2 software package were used [20]. The reference results were compared on the basis of the maximum relative error obtained for numerous simulations (ε = 1.40%).

Finally, the objective in this work was to investigate the effect of the Damköhler number (Da) and Reynolds number (Re) on the laminar flow in a channel with an open square cavity and a reactive bottom wall in two dimensions in a first-order chemical reaction using the LBM. For the numerical simulations, we developed a custom code in Fortran 90, specifically designed and implemented for the Ph.D. project of Burgos-Vergara [21]. The code was built from the ground up to provide a flexible and efficient framework for simulating fluid dynamics using the LBM. The code allows for the adjustment and optimization of key parameters, such as the Reynolds and Damköhler numbers, enabling detailed and accurate simulations under various conditions [21,22]. The validity of the code was rigorously assessed through multiple simulation cases, including comparisons with the results obtained from established commercial software and analytical solutions. This validation process ensures the robustness and reliability of the approach. Furthermore, the results obtained from the custom code were validated against benchmark data from the literature, particularly the work by Burgos-Vergara et al. [22], which presents a numerical study of laminar mixed convection in a square open cavity. The validation also involved comparisons with results from commercial software solutions to further confirm the accuracy of the simulations.

2. Materials and Methods

2.1. Numerical Method—Lattice Boltzmann Equation

The LBM is an alternative computational method for simulating fluid flow. It is a predecessor to the lattice gas automata, which were developed from the lattice gas automaton in the 1990s to solve the Navier–Stokes equation [1,23,24]. This method is based on the discretization of the Boltzmann equation in time and space so that the set of discretized velocity distribution functions $f_i(x,t)$ for the momentum and $A_i(x,t)$, $B_i(x,t)$ for the reaction field of species evolve, propagating from node to node in each time step. Specifically, the LBM is performed in two main steps: during the propagation step, the particles are forced to move along prescribed lattice directions, whereas the collision step imposes thermalization with a characteristic time scale after one mean free path.

2.2. Velocity Discretizations for the LBM

Different velocity discretizations for the LBM have been developed; D2Q9 is the discretization most commonly used for simulations of two-dimensional momentum trans-

fer [25,26], whereas D2Q4 and D2Q9 are commonly used for the discretization of the temperature, chemical reaction and momentum fields [27,28]. In the present work, we used D2Q9 for both the momentum and the chemical reaction grids. The BGK model with SRT, which is the model usually applied, is sufficient to ensure the stability of the momentum transfer for the range of Reynolds numbers and Damköhler numbers in our problem. The BGK model with SRT is usually applied in such cases [10,15]. The distribution functions for the SRT LBM on a D2Q9 grid are calculated in the following form to solve the momentum equation:

$$f_i(x + \boldsymbol{c}_i\Delta t, t + \Delta t) = f_i(x,t) + \frac{1}{\tau}[f_i^{eq}(x,t) - f_i(x,t)] \quad (1)$$

where f_i is the momentum distribution function, and c_i represents the discretized unitary velocities of the D2Q9 model, $\boldsymbol{c}_0(0, 0)$, $\boldsymbol{c}_1(1, 0)$, $\boldsymbol{c}_2(0, 1)$, $\boldsymbol{c}_3(-1, 0)$, $\boldsymbol{c}_4(0, -1)$, $\boldsymbol{c}_5(1, 1)$, $\boldsymbol{c}_6(1, 1)$, $\boldsymbol{c}_7(1, 1)$ and $\boldsymbol{c}_8(1, 1)$, as shown in Figure 1.

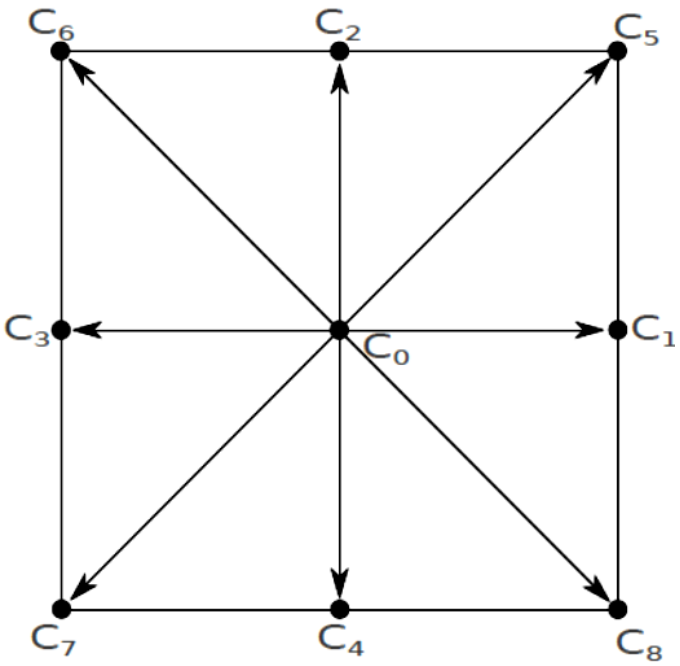


Figure 1. D2Q9 model, lattice velocities.

The parameter τ is the dimensional relaxation time that controls the rate at which equilibrium for the momentum is approached. The kinematic viscosity v is directly related to the relaxation time parameter τ. These parameters control the stability of the method and are defined in terms of their respective relaxation times [29,30]. The macroscopic viscosity is calculated as follows:

$$v = \left(\tau\frac{1}{2}\right)c_s^2\Delta t \quad (2)$$

where $c_s = c/\sqrt{3}$ is the lattice speed of sound, and $c = \Delta x/\Delta t$ (Δx and Δt are the lattice space and the lattice time step size, which are set to unity). The equilibrium distribution functions for momentum f_i^{eq} are given by the following:

$$f_i^{eq} = \omega_i\rho\left[1 + 3\frac{\boldsymbol{c}_i.\mathbf{u}}{c^2} + \frac{9}{2}\frac{\left(\boldsymbol{c}_i.\mathbf{u}\right)^2}{c^4} - \frac{3}{2}\frac{\mathbf{u}.\mathbf{u}}{c^2}\right] \quad (3)$$

where ρ is the local material density, u is the macroscopic velocity and ω_i represents the weights of the D2Q9 model: 4/9 for i = 0; 1/9 for i = 1, 3, 5, 7; and 1/36 for i = 2, 4, 6, 8 [2]. The distribution functions include information about the macroscopic properties (e.g.,

density, velocity, temperature and concentration). Therefore, $f_i(x,t)$ can be used to compute all of the macroscopic variables, such as density ρ and velocity u, which are calculated as follows:

$$\rho(x,t) = \sum_{i=0}^{8} f_i(x,t) \;\; \rho\mathbf{u}(x,t) = \sum_{i=0}^{8} \boldsymbol{c}_i f_i(x,t) \tag{4}$$

For the concentration fields, two new distribution functions must be used [29,30]. The LBM equations for species A and B for the D2Q9 model are then expressed as follows:

$$A_i(x + \boldsymbol{c}_i\Delta t, t + \Delta t) = A_i(x,t) + \frac{1}{\tau_A}[A_i^{eq}(x,t) - A_i(x,t)] - S_y \tag{5}$$

$$B_i(x + \boldsymbol{c}_i\Delta t, t + \Delta t) = B_i(x,t) + \frac{1}{\tau_B}[B_i^{eq}(x,t) - B_i(x,t)\,] + S_y \tag{6}$$

where A_i and B_i are the distribution function equations for the mass transfer of species A and B, respectively. The source term S_y in the distribution function of A_i is negative to express that the consumption of reactant A corresponds to the generation of product B. The source term is calculated as follows [31]:

$$S_y = \omega_i \, kC^A \tag{7}$$

where k is the reaction constant, and C^A and C^B are the concentrations of reactant A and product B, respectively. The macroscopic mass diffusivity D^σ is directly related to the relaxation time parameters τ_A and τ_B for each lattice grid and is calculated as follows:

$$D^\sigma = \left(\tau_\sigma \frac{1}{2}\right) c_s^2 \Delta t; \; \sigma = (A, \; B) \tag{8}$$

The index σ refers to the different species, and the equilibrium distribution functions A_i^{eq}, B_i^{eq} are defined by the following:

$$A_i^{eq} = \omega_i \, C^A \left[1 + \frac{\boldsymbol{c}_i.\mathbf{u}}{c^2}\right] \tag{9}$$

$$B_i^{eq} = \omega_i \, C^B \left[1 + \frac{\boldsymbol{c}_i.\mathbf{u}}{c^2}\right] \tag{10}$$

2.3. Boundary Conditions

For boundary conditions, the velocity is specified at the inlet as a uniform flow field along the channel direction, and the Dirichlet condition is treated using the Zou–He approach [32,33]. The outlet open boundary condition is used, and full-way bounce-back is used for the rest of the solid boundaries (north and south) and the other walls of the cavity [27]. The concentration of the species can be calculated using the following equations:

$$C^A(x,t) = \sum_{i=0}^{8} A_i(x,t) \tag{11}$$

$$C^B(x,t) = \sum_{i=0}^{8} B_i(x,t) \tag{12}$$

3. Results and Discussion

3.1. Physical Problem

During the course of the reaction, reactant A is consumed when it contacts the reaction at the plate, where product B is generated. We assume isothermal conditions and a reaction–

diffusion dynamic, where both species are simply advected by an external flow. The geometry of the problem consists of an open cavity with external flow and with the reaction at the plate located at the bottom wall of the cavity, as shown in Figure 2.

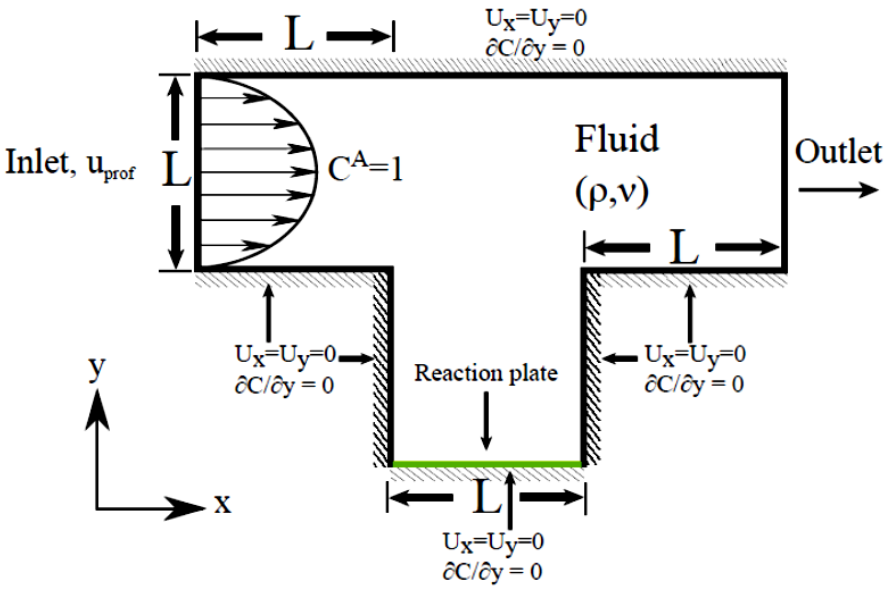


Figure 2. A scheme of the open cavity with a reactive bottom plate.

The reaction rate is determined through the measurement of concentration, either when the concentration of A decreases or the concentration of B increases. The consumption of reactant A is expressed in the following form:

$$R = -kC^A \tag{13}$$

where k is the reaction constant, and C^A and C^B are the concentrations of reactant A and product B, respectively. The flow field is modeled via the LBM with the D2Q9 model. For the concentration field of species A and B, two new lattice meshes for the mass transfer processes are required, along with two new transport equations for the distribution functions of both species. Additionally, a term for the chemical reactions (S_y) is added as a source, which accounts for the rate of production of species B.

3.2. Dimensionless Parameters

The dimensionless parameter characteristic of the problem is the Damköhler number Da, which is defined as the ratio between the reaction rate and the diffusion rate:

$$Da = \frac{k\delta}{DA} \tag{14}$$

where δ is the characteristic length of the reaction plate, k is the convective mass transfer coefficient and DA is the diffusion coefficient of species A. The Péclet number Pe can be determined through a relation between the Reynolds number Re and the Schmidt number Sc as $Pe = ReSc$, where Sc is defined as $Sc = v/D$. Specifically, the Schmidt number is the ratio between kinematic viscosity and the mass diffusivity D of the substance in the medium. For instance, the mass diffusivity of CO_2 in air is $D_{CO_2} = 19 \times 10^{-6}$, and the Schmidt number is $Sc = 1.14$. The value of Sc was fixed at $S_{CA} = S_{CB} = 1$. The reaction

rate k can be determined from Da to obtain the source term S_y in Equation (8); this term is needed in Equations (6) and (7) for A_i and B_i:

$$k = \frac{Da.\,DA}{\delta} \tag{15}$$

Subsequently, the diffusion coefficient is determined by the following:

$$DA = \frac{u.\,\delta}{Pe} \tag{16}$$

where u is the characteristic flow velocity; the Péclet number (Pe) is calculated from $Pe = Re.Sc$ for species A and B, for Re = 1, 2, 5, 7, 10 and Da = 1. The mass transfer per unit length is characterized by the Sherwood number Sh, which is a dimensionless parameter. The Sherwood number appears in many correlations, depending on the geometry, in combination with other dimensionless parameters (e.g., Re or Sc). Several correlations in the literature can be used for a quick comparison of the results [34,35]. For example, Sh can be calculated according to the following correlation:

$$Sh = \frac{k\,L}{D_f} = 0.664 Re_L^{1/2}.\,Sc^{1/3} \tag{17}$$

where D_f is the diffusion coefficient of the component in the fluid, and L is the characteristic length of the system. The Reynolds number Re_L is based on the length of the flat plate (i.e., the catalysis region). Meanwhile, the Sherwood number Sh is analogous to the Nusselt number Nu for heat transfer processes and can be expressed through the gradient of the dimensionless concentration on the flat plate. Thus,

$$Sh = \frac{k\,L}{D_f} = \frac{\partial C}{\partial Y}\,[react - wall] \tag{18}$$

The average Sherwood number ($\overline{Sh}$) is calculated as follows:

$$\overline{Sh} = \frac{1}{L}\int_0^L Sh\,dy. \tag{19}$$

3.3. The Effect of the Reynolds Number on Concentrations

Figure 3 displays the contours of the dimensionless concentrations of A and B for a Damköhler number equal to 1 and different Reynolds numbers. The generation of B is controlled by Da for Equation (15). The effect of the Reynolds number in the cavity is such that the material diffusion of B into the channel decreases with increasing Re (Figure 3a–e); the concentration of product B is then reduced.

Figure 4 shows a plot of the concentrations of species A (C_A) and B (C_B) in the center of the cavity as a function of time. For Re = 1, the saturation concentration occurs as product B reaches a value of 0.52, and the remaining reactant A reaches a value of 0.48 (Figure 4a). For Re = 10, the maximum concentration of product B decreases to 0.37, whereas the concentration of A saturates at 0.63, as shown in Figure 4e,f.

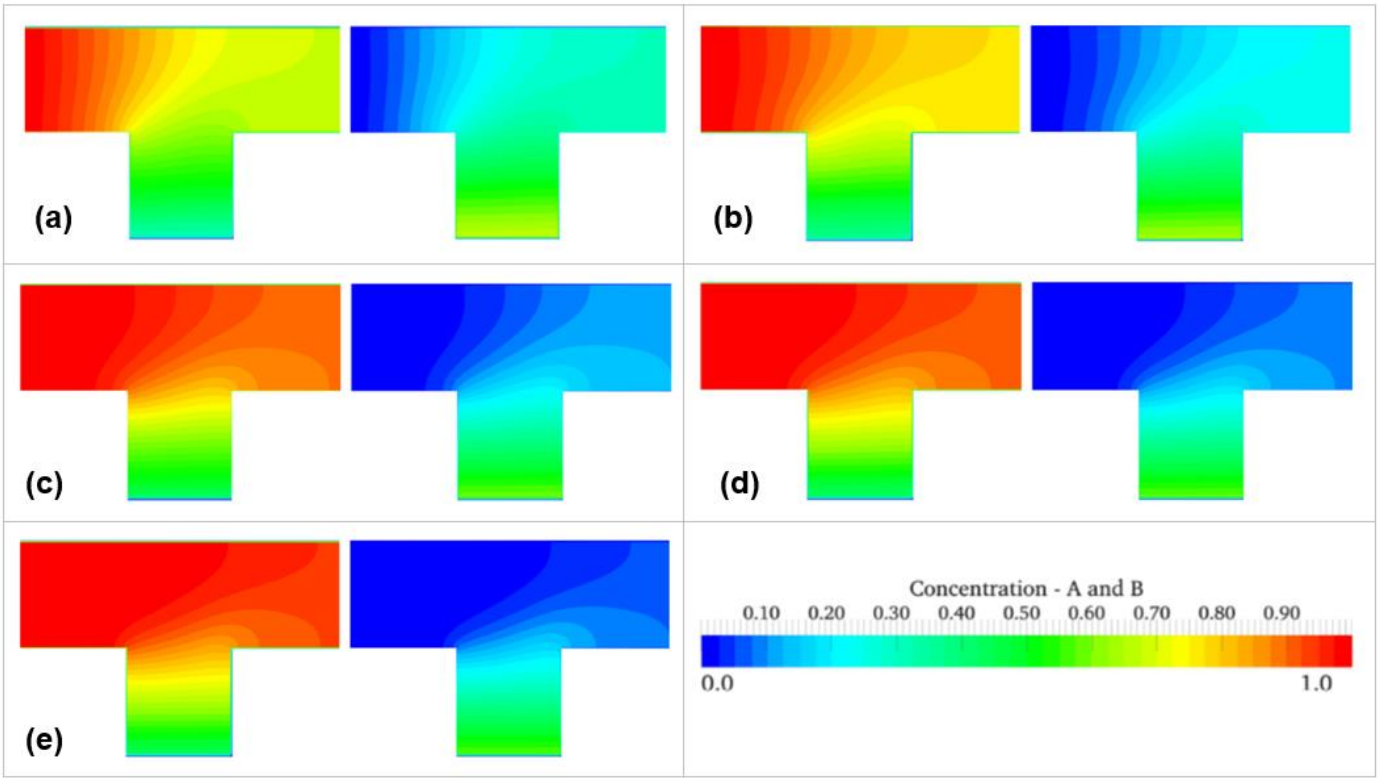


Figure 3. Steady-state dimensionless concentration for reactant A (**left**) and product B (**right**), for Da = 1 and Re = 1 (**a**), Re = 2 (**b**), Re = 5 (**c**), Re = 7 (**d**) and Re = 10 (**e**).

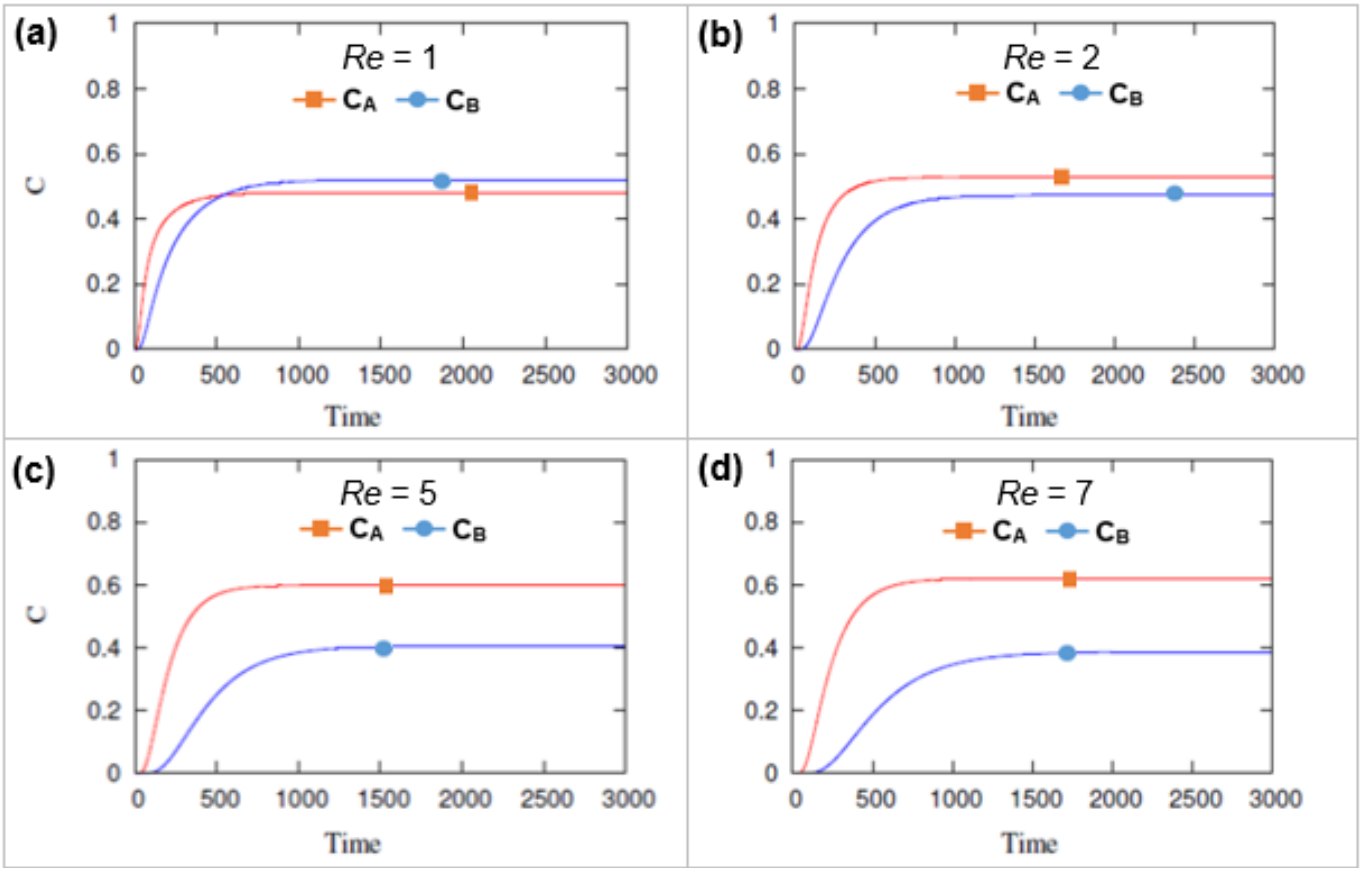


Figure 4. *Cont*.

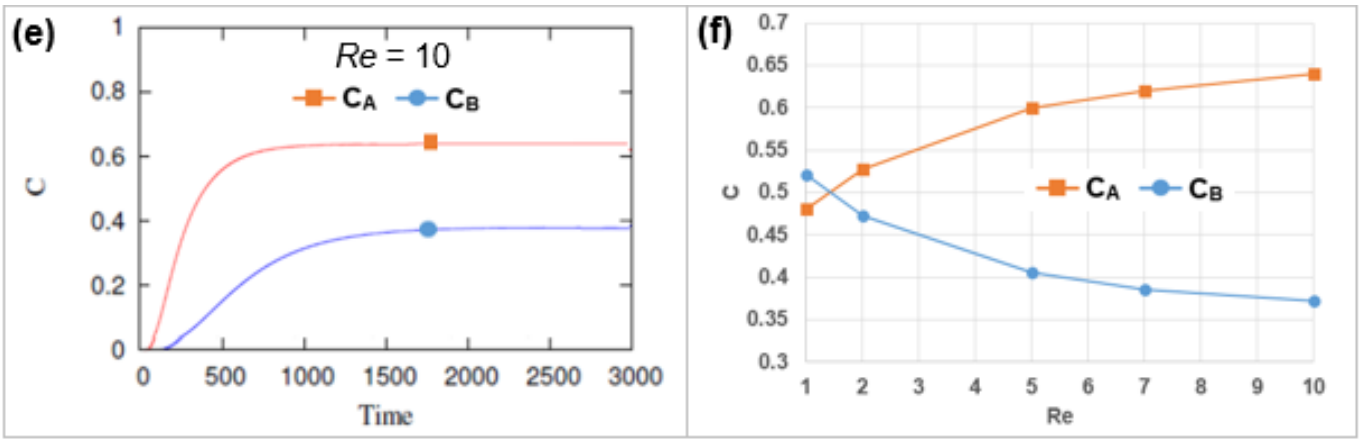


Figure 4. A plot of the dimensionless concentration of A and B along time measured in the center of the cavity for Da = 1 and Re = 1 (**a**), Re = 2 (**b**), Re = 5 (**c**), Re = 7 (**d**) and Re = 10 (**e**) and concentration as a function of Re (**f**).

3.4. The Effect of the Damköhler Number on Concentrations

Figure 5 displays the results of different simulations conducted using different Damköhler numbers, Da = 0.1, 1.0, 10, 100. The Reynolds number was fixed at Re = 5 to observe the effect of the Damköhler number in the production of substance B. As evident in Figure 5a–d, an increase in Da caused the concentration of B to increase (and the concentration of A to correspondingly decrease) in both the cavity and the channel.

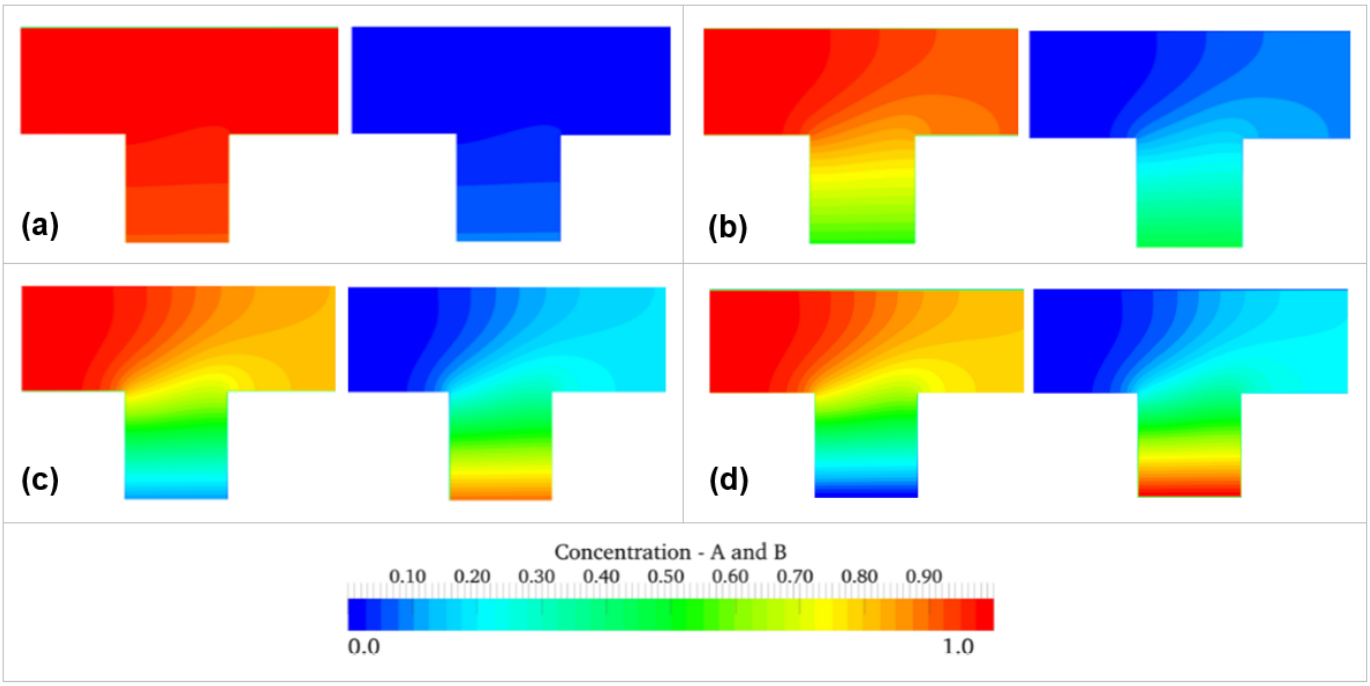


Figure 5. Steady-state dimensionless concentration for reactant A (**left**) and product B (**right**) for Re = 5 and Damköhler number Da = 0.1 (**a**), Da = 1 (**b**), Da = 10 (**c**) and Da = 100 (**d**).

Combining the results for Da = 0.1 (Figure 5a) with those for Da = 100 (Figure 5d) reveals that, in the first case, the reaction is much slower, and the production of B reaches a maximum value of 0.06 in the center of the cavity. In the case of Da = 100, the reaction is much faster, and reactant A is absorbed almost entirely. Notably, the concentration of product B (CB) reaches a maximum at 0.66 in the center of the cavity, as shown in Figure 6d,e.

Consequently, a Damköhler number in the range $0.1 < Da \leq 100$ and a Reynolds number in the range $1 \leq Re \leq 10$ control the reaction rate on the reactive wall.

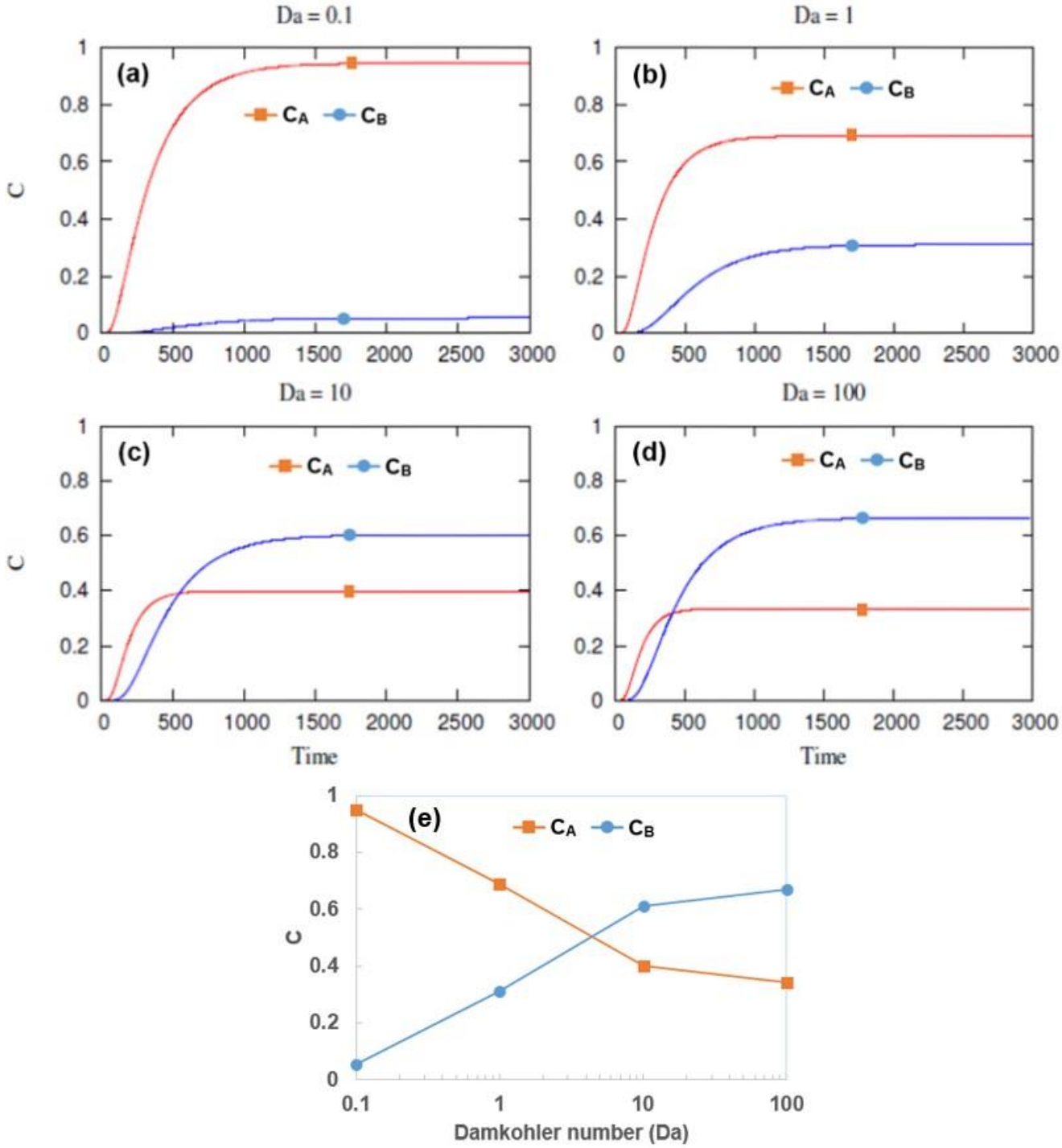


Figure 6. The dimensionless concentration of A and B in the middle of the cavity for Re = 5 and Da = 0.1 (**a**), Da = 1.0 (**b**), Da = 10 (**c**) and Da = 100 (**d**) and concentration as a function of Da (**e**).

3.5. Effect of Damköhler Number on Sherwood Number

Finally, Figure 7 displays the value of the average Sherwood number for product B measured on the reaction plate at the bottom of the cavity for different Damköhler numbers (Da = 0.1, 1.0, 10, 100). The average Sherwood number increases as a function of the increase in the Damköhler number, rapidly for Da varying between 0.1 and 10 (Figure 7a–c), and reaches stability for variations in Da greater than 10 (Figure 7e).

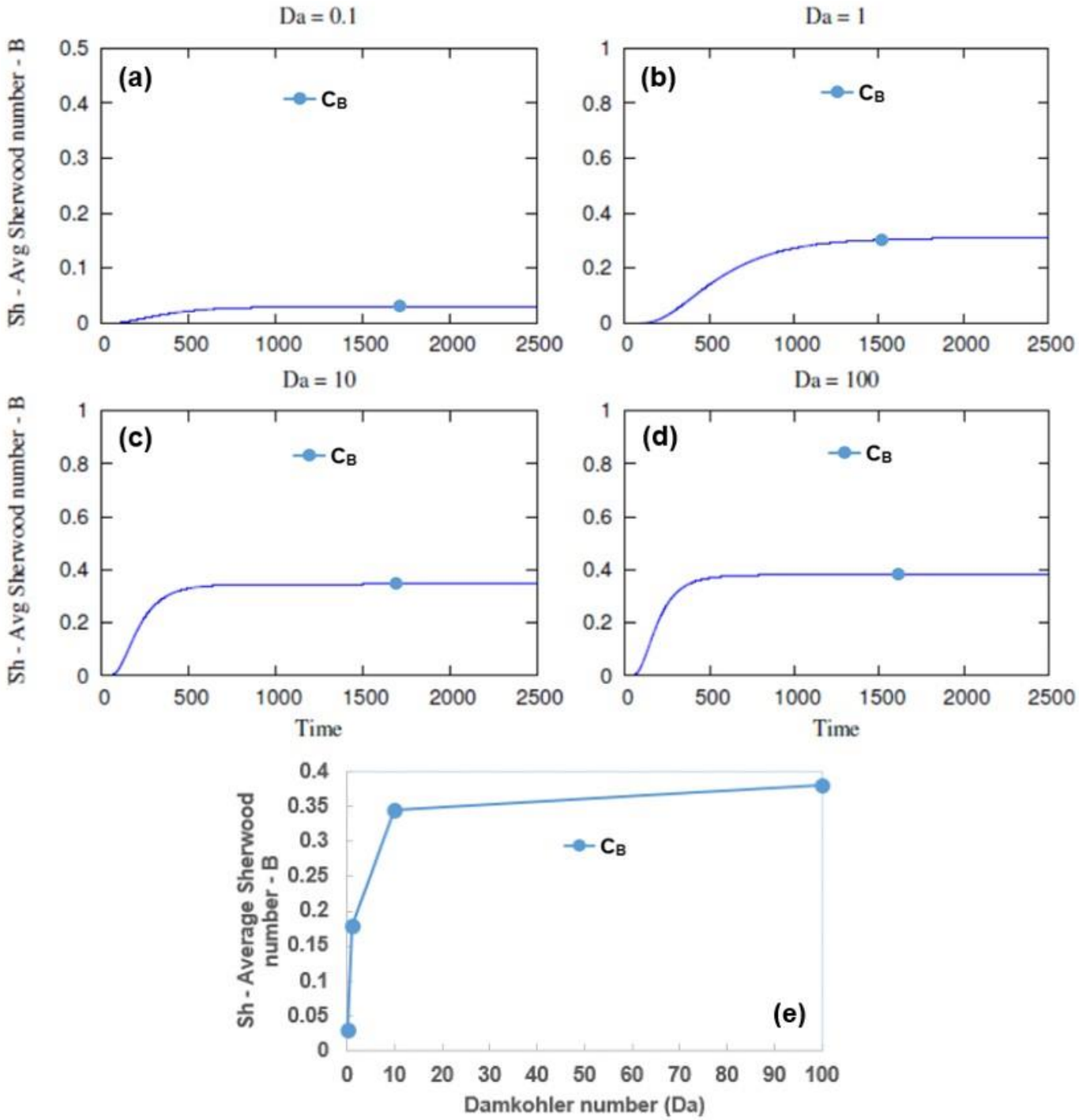


Figure 7. The average Sherwood number for product *B* measured on the reaction plate at the bottom of the cavity, for *Re* = 5 and *Da* = 0.1 (**a**), *Da* = 1.0 (**b**), *Da* = 10 (**c**) and *Da* = 100 (**d**) and the average Sherwood number as a function of *Da* (**e**).

4. Conclusions

Numerical simulations of a first-order chemical reaction in an open square cavity were carried out using SRT collision models (D2Q9) to study the effect of variations in the Reynolds number (Re) and Damköhler number (Da) with a concentration flow in two dimensions. Study flows were analyzed in the incompressible limit as a function of the Reynolds and Damköhler numbers. In the first case, the Damköhler number was fixed at 1, and different Reynolds number values were used (Re = 1, 2, 5, 7, 10). We observed that the generation of product B was controlled for the Damköhler number. The effect of the

Reynolds number was considerable inside of the cavity, such that the diffusion of product B in the channel decreased with increasing Re as a result of the concentration of B decreasing as a consequence of the reaction velocity controlled by Da being low with respect to the flow velocity. In addition, because reactant A did not achieve a complete reaction in the bottom of the cavity, some of reactant A was carried away by the channel flow. For Re = 10, we obtained an increase in the concentration of reactant A, which reached a maximum value of 0.63 inside of the cavity; the concentration of product B reached a maximum value of 0.37.

Author Contributions: Conceptualization, J.B.-V. and C.Y.Q.-C.; methodology, J.B.-V.; software, J.B.-V.; writing—original draft preparation, J.B.-V. and C.Y.Q.-C.; writing—review and editing, J.B.-V., C.Y.Q.-C., M.M.S.-C. and A.I.V.-A. All authors have read and agreed to the published version of the manuscript.

Funding: This research received no external funding.

Data Availability Statement: The data presented in this study are available on request from the corresponding author.

Acknowledgments: The authors are grateful for the support of the project SAT-INV-2398 financed by the Universidad Cooperativa de Colombia—UCC—within the ISI Research Group.

Conflicts of Interest: The authors declare no conflicts of interest.

References

1. Tao, S.; Xu, A.; He, Q.; Chen, B.; Qin, F.G.F. A Curved Lattice Boltzmann Boundary Scheme for Thermal Convective Flows with Neumann Boundary Condition. *Int. J. Heat Mass Transf.* **2020**, *150*, 119345. [CrossRef]
2. Luo, L.-S. Lattice-Gas Automata and Lattice Boltzmann Equations for Two-Dimensional Hydrodynamics. Ph.D. Thesis, Georgia Institute of Technology, Atlanta, GA, USA, 1993.
3. Martins, I.T.; Alvariño, P.F.; Cabezas-Gómez, L. Lattice Boltzmann Method for Simulating Transport Phenomena Avoiding the Use of Lattice Units. *J Braz. Soc. Mech. Sci. Eng.* **2024**, *46*, 333. [CrossRef]
4. Nabavizadeh, S.A.; Barua, H.; Eshraghi, M.; Felicelli, S.D. A Multiple-Grid Lattice Boltzmann Method for Natural Convection under Low and High Prandtl Numbers. *Fluids* **2021**, *6*, 148. [CrossRef]
5. Samanta, R.; Chattopadhyay, H. Simulation of Corner Solidification in a Cavity Using the Lattice Boltzmann Method. *Fluids* **2024**, *9*, 195. [CrossRef]
6. Han, M.; Kikumoto, H.; Ooka, R. Numerical Investigation of Lattice Boltzmann Method-Based Large-Eddy Simulation in Non-Isothermal Enclosed Cavity Airflow. *Int. Commun. Heat Mass Transf.* **2024**, *157*, 107698. [CrossRef]
7. Lourenço, R.G.C.; Friggo, J.R.; Constantino, P.H.; Tavares, F.W. The Lattice Boltzmann Method for Mass Transfer of Miscible Multicomponent Mixtures: A Review. *Phys. Fluids* **2024**, *36*, 061302. [CrossRef]
8. Zulfiqar, U.; Haider, F.U.; Ahmad, M.; Hussain, S.; Maqsood, M.F.; Ishfaq, M.; Shahzad, B.; Waqas, M.M.; Ali, B.; Tayyab, M.N.; et al. Chromium Toxicity, Speciation, and Remediation Strategies in Soil-Plant Interface: A Critical Review. *Front. Plant Sci.* **2023**, *13*, 1081624. [CrossRef]
9. Haussmann, M.; Reinshaus, P.; Simonis, S.; Nirschl, H.; Krause, M.J. Fluid–Structure Interaction Simulation of a Coriolis Mass Flowmeter Using a Lattice Boltzmann Method. *Fluids* **2021**, *6*, 167. [CrossRef]
10. Bhatnagar, P.L.; Gross, E.P.; Krook, M. A Model for Collision Processes in Gases. I. Small Amplitude Processes in Charged and Neutral One-Component Systems. *Phys. Rev.* **1954**, *94*, 511–525. [CrossRef]
11. Mezrhab, A.; Amine Moussaoui, M.; Jami, M.; Naji, H.; Bouzidi, M. Double MRT Thermal Lattice Boltzmann Method for Simulating Convective Flows. *Phys. Lett. A* **2010**, *374*, 3499–3507. [CrossRef]
12. Huang, R.; Wu, H. A Modified Multiple-Relaxation-Time Lattice Boltzmann Model for Convection–Diffusion Equation. *J. Comput. Phys.* **2014**, *274*, 50–63. [CrossRef]
13. Muthukumaran, R.; Mishra, S.C. Effects of the Incidence of a Gaussian Temporal Short-Pulse Laser of Different Spatial Profiles on a Two-Dimensional, Rectangular, Inhomogeneous Participating Medium. *Numer. Heat Transf. Part A Appl.* **2008**, *54*, 525–545. [CrossRef]
14. Yu, H.; Luo, L.-S.; Girimaji, S.S. LES of Turbulent Square Jet Flow Using an MRT Lattice Boltzmann Model. *Comput. Fluids* **2006**, *35*, 957–965. [CrossRef]

15. Gehrke, M.; Janßen, C.F.; Rung, T. Scrutinizing Lattice Boltzmann Methods for Direct Numerical Simulations of Turbulent Channel Flows. *Comput. Fluids* **2017**, *156*, 247–263. [CrossRef]
16. Lu, J.H.; Lei, H.Y.; Dai, C.S. Analysis of Henry's Law and a Unified Lattice Boltzmann Equation for Conjugate Mass Transfer Problem. *Chem. Eng. Sci.* **2019**, *199*, 319–331. [CrossRef]
17. Poureslami, P.; Siavashi, M.; Moghimi, H.; Hosseini, M. Pore-Scale Convection-Conduction Heat Transfer and Fluid Flow in Open-Cell Metal Foams: A Three-Dimensional Multiple-Relaxation Time Lattice Boltzmann (MRT-LBM) Solution. *Int. Commun. Heat Mass Transf.* **2021**, *126*, 105465. [CrossRef]
18. Valle, N.; Haverkort, J.W. Analytical Mass Transfer Coefficients for Natural Convection from Vertical Gas-Evolving Electrodes. *Int. J. Heat Mass Transf.* **2024**, *225*, 125390. [CrossRef]
19. Holzbecher, E. Numerical Solutions for the Lévêque Problem of Boundary Layer Mass or Heat Flux. In Proceedings of the European COMSOL Conference, Hannover, Germany, 4–6 November 2008; COMSOL: Berlin, Germany, 2008.
20. Albrand, P.; Lalanne, B. Mass Transfer Rate in Gas-Liquid Taylor Flow: Sherwood Numbers from Numerical Simulations. *Chem. Eng. Sci.* **2023**, *280*, 119011. [CrossRef]
21. Burgos Vergara, J. Numerical Study of the Heat and Mass Transfer Processes with the Lattice Boltzmann Method: Laminar Mixed Convection in a Square Open C. Ph.D. Thesis, Universitat Rovira i Virgili, Tarragona, Spain, 2016.
22. Burgos, J.; Cuesta, I.; Salueña, C. Numerical Study of Laminar Mixed Convection in a Square Open Cavity. *Int. J. Heat Mass Transf.* **2016**, *99*, 599–612. [CrossRef]
23. Wolf-Gladrow, D.A. 1. Introduction. In *Lattice Gas Cellular Automata and Lattice Boltzmann Models: An Introduction*; Wolf-Gladrow, D.A., Ed.; Springer: Berlin, Heidelberg, 2000; pp. 1–13, ISBN 978-3-540-46586-7.
24. Chen, S.; Doolen, G.D. Lattice Boltzmann Method for Fluid Flows. *Annu. Rev. Fluid Mech.* **1998**, *30*, 329–364. [CrossRef]
25. Xia, M.; Zhou, H.; Jiang, C.; Cui, J.; Zeng, Y.; Chen, H. Comparative Study of 2D Lattice Boltzmann Models for Simulating Seismic Waves. *Remote Sens.* **2024**, *16*, 285. [CrossRef]
26. Kossov, V.; Zhakebayev, D.; Fedorenko, O.; Zhumali, A. Distinctions of the Emergence of Convective Flows at the "Diffusion–Convections" Boundary in Isothermal Ternary Gas Mixtures with Carbon Dioxide. *Fluids* **2024**, *9*, 47. [CrossRef]
27. Mohamad, A.A. The Boltzmann Equation. In *Lattice Boltzmann Method: Fundamentals and Engineering Applications with Computer Codes*; Mohamad, A.A., Ed.; Springer: London, UK, 2011; pp. 15–24, ISBN 978-0-85729-455-5.
28. Mohamad, A.A.; El-Ganaoui, M.; Bennacer, R. Lattice Boltzmann Simulation of Natural Convection in an Open Ended Cavity. *Int. J. Therm. Sci.* **2009**, *48*, 1870–1875. [CrossRef]
29. Barrios, G.; Rechtman, R.; Rojas, J.; Tovar, R. The Lattice Boltzmann Equation for Natural Convection in a Two-Dimensional Cavity with a Partially Heated Wall. *J. Fluid Mech.* **2005**, *522*, 91–100. [CrossRef]
30. Lin, K.-H.; Liao, C.-C.; Lien, S.-Y.; Lin, C.-A. Thermal Lattice Boltzmann Simulations of Natural Convection with Complex Geometry. *Comput. Fluids* **2012**, *69*, 35–44. [CrossRef]
31. Delavar, M.A.; Farhadi, M.; Sedighi, K. Numerical Simulation of Direct Methanol Fuel Cells Using Lattice Boltzmann Method. *Int. J. Hydrogen Energy* **2010**, *35*, 9306–9317. [CrossRef]
32. Zou, Q.; He, X. On Pressure and Velocity Boundary Conditions for the Lattice Boltzmann BGK Model. *Phys. Fluids* **1997**, *9*, 1591–1598. [CrossRef]
33. Frihat, M.; Podvin, B.; Mathelin, L.; Fraigneau, Y.; Yvon, F. Coherent Structure Identification in Turbulent Channel Flow Using Latent Dirichlet Allocation. *J. Fluid Mech.* **2021**, *920*, A27. [CrossRef]
34. Welty, J.; Rorrer, G.L.; Foster, D.G. *Fundamentals of Momentum, Heat, and Mass Transfer*; John Wiley & Sons: Hoboken, NJ, USA, 2014; ISBN 978-1-118-94746-3.
35. Edgar, T.F.; Felder, R.M.; McKenna, J.; Rousseau, R.W.; Sandier, S.I.; Seagrave, R.C. *Bird, Stewart and Lightfoot: Transport Phenomena*, 2nd ed.; Wiley India Pvt. Limited: Singapore, 2006; ISBN 978-81-265-0808-2.

Disclaimer/Publisher's Note: The statements, opinions and data contained in all publications are solely those of the individual author(s) and contributor(s) and not of MDPI and/or the editor(s). MDPI and/or the editor(s) disclaim responsibility for any injury to people or property resulting from any ideas, methods, instructions or products referred to in the content.